ELSEVIER

Journal of Power Sources 104 (2002) 208–220

JOURNAL OF POWER SOURCES

www.elsevier.com/locate/jpowsour

Characterisation of separator papers for use in valve regulated lead/acid batteries

R.J. Ball[a,*], R. Evans[b], R. Stevens[a]

[a]*Department of Engineering and Applied Science, University of Bath, Bath BA2 7AY, UK*
[b]*Invensys, Westinghouse site, Chippenham, Wiltshire SN15 1SJ, UK*

Received 2 July 2001; received in revised form 3 September 2001; accepted 3 September 2001

Abstract

Separator papers are an essential component of a valve regulated lead/acid (VRLA) battery. In addition to separating the positive and negative electrodes, they provide a constant pressure on the active materials thereby reducing the rate of degradation during cycling. Dendrites formed from the negative active material are also less likely to cause short circuits in batteries where a separator is employed. The level to which a separator will influence the performance of a VRLA battery it strongly dependent on its properties. This paper describes the results from a series of tests used to characterise the properties of separators most influential to battery performance. These properties include, the macroscopic structure, permittivity and wicking rates. During the operational life of a VRLA battery the volume of electrolyte will decrease, due mainly to the electrolysis of water during overcharging. The consequence of this process is a variation of acid saturation during the life of the battery, which will have a direct influence on the compressive and diffusive properties of the separator. Compressive and diffusive characteristics were therefore measured over a range of saturation levels. Characterisation was conducted on three separator types. Types A and B were 100% glass but had slightly different structures and type C contained 8% polyester fibres mixed with glass.

Keywords: Separator paper; Diffusivity; VRLA

1. Introduction

Separator papers play an important role in the operation of a valve regulated lead/acid (VRLA) battery in several ways. In addition to providing a means by which to immobilise the electrolyte and prevent positive and negative plates from coming into contact with each other, they can influence the reactions occurring within the battery. The behaviour of a separator paper in the environment of a battery is directly related to its structure. Battery separator structures are complex and characterised using a wide range of different techniques. Currently used methods can be divided into two groups, each concerned with a different aspect of the influence of separators on battery operation.

The first of these is concerned with the flow of liquid or gas through the paper, which include wicking, drainage and diffusion tests. Culpin [1] has examined these characteristics in some detail. He investigated the drainage characteristics of separators in both the free and compressed state. Testing in the compressed state simulates the forces exerted by the cell walls through the electrodes on the separator. Paper saturation was calculated from the dimensions and weight difference of the papers between the saturated and dry state.

The second type of test evaluates the behaviour of the separator whilst under a compressive load [2,3]. This is normally combined with measurement of the change in force or strain associated with variations in paper saturation. This is relevant as changes in saturation occur as a result of electrolyte water loss during cycling.

There is no universally agreed standard method for the determination of a simple parameter such as separator thickness. Both 'The Battery Council International' (BCI) and 'The Japanese Industrial Standards' (JIS) propose different methods. The BCI utilise a 29 mm anvil and 10.34 kPa load, whereas the JIS use 10 cm × 10 cm samples with a 20 kPa load [4]. These different test methods can give variations in measured parameters of up to 20% for the same material. It is therefore important to only use one test protocol when designing batteries. The compressive force exerted on the battery plates by the separator will be

* Corresponding author. Tel.: +44-01225-826826; fax: +44-01225-826098.
E-mail address: r.j.ball@bath.ac.uk (R.J. Ball).

0378-7753/02/$ – see front matter
PII: S0378-7753(01)00925-9

influenced by a number of factors, which must be taken into account in battery design. The most significant of these are as follows [5]:

- how thickness is measured;
- variation in separator materials;
- variation of the plate dimensions;
- draught on battery case;
- separator compression used (restrained thickness/unrestrained thickness);
- acid saturation level;
- density of separator;
- surface area of separator;
- case material used;
- uniformity of compression between plates.

When considering the problem of characterising a more complex property such as behaviour under compressive loading, whilst saturated with electrolyte, there is even more opportunity to vary procedures. For example, the viscoelastic properties of the paper will influence results depending on what load rate is used. Sample dimensions can also affect results.

Nakamura et. al. [2] have studied the compressive properties of separators using a jig, where a stack of five separator papers are mounted horizontally between two plates. The distance between the plates is variable and measurements of the load were taken via a load cell. Samples were compressed to a specified load and then the acid added after a period of 1 hour had elapsed. In comparison, an alternative approach adopted by McGregor [3] utilised a specially designed piston cell. This consisted of a normal battery cell with one of the walls connected to a piston therefore allowing variations in cell compression to be made. Separator papers were held in the vertical position and dividing plates inserted between the papers. Compressive loads were applied and measured using a pressure gauge attached to a regulated gas supply and the cell piston.

Results from both researchers indicated the general trend of a reduction in thickness or force applied by the paper as saturation was increased from 0%. However, results from Nakamura, suggest a reversal of this trend and an increase in force after a saturation of approximately 50% is reached.

This paper describes results obtained from the characterisation of three separator paper types using a range of techniques.

2. Experimental methods

2.1. Scanning electron microscopy

Samples of each separator type studied were examined in a JEOL 6310 scanning electron microscope. In order to prevent charging of the glass fibres a thick layer of gold was applied using an Edwards sputter coater.

2.2. Wicking measurements

The rate at which an electrolyte rises up a sample of separator paper by capillary action will be influenced by both separator structure and material. It is extremely difficult to model the flow of electrolyte through a fibrous material such as a separator; however, if the pores are assumed to be round in cross-section the wicking characteristics can be described using the Washburn equation. The equation relates the velocity of the liquid, v ($\mathrm{d}h/\mathrm{d}t$), at a given height, h, to pore radius, r, surface tension, γ, contact angle between liquid and solid surface, θ, viscosity, η, density, ρ, and the gravitational constant, g. The equation is generally written in the following form [1]:

$$v = \frac{\mathrm{d}h}{\mathrm{d}t} = \frac{2r\gamma\cos\theta}{8\eta h} - \frac{r^2\rho g}{8\eta} \quad (1)$$

integration of Eq. (1) ignoring the gravity term yields Eq. (2), where K is tortuosity [1].

$$h^2 = \frac{\gamma r t\cos\theta}{K^2 2\eta} \quad (2)$$

Eq. (2) predicts that for values of $h \ll h_\mathrm{m}$, where h_m is the maximum height reached, at infinite time, the relationship between h^2 and t is linear [6]. Wicking characteristics of different separator papers were compared by plotting height squared, h^2, versus time, t, within the saturation range where the gradient is proportional to the wicking rate.

Wicking tests were conducted using separator paper strips of 20 mm × 155 mm. Separator paper is manufactured as strip (or roll) using a continuous process. Samples were cut at 0 degrees and at 90 degrees to the manufacturing direction of the paper. Dots of saturated methyl red indicator solution in ethanol were applied at 10 mm intervals along the length of the strip, starting 5 mm from one end. Methyl red is orange when neutral and turns to a deep red on contact with acid thus allowing the electrolyte front to be clearly visible.

Each strip was suspended in electrolyte so that the meniscus was level with the first dot 5 mm from the strip end. The time the electrolyte front reached each dot was then recorded until the strip was totally saturated and all the dots had changed colour.

2.3. Permeability

The pore size distribution of the materials was determined using a liquid displacement method. This method relies on the principle that there is a rise of liquid in a capillary due to surface tension. At equilibrium, the following expression can be written for liquid rising up a capillary.

$$2\pi r\gamma\cos\theta = r^2\pi h\rho g \quad (3)$$

Capillary or pore radius, r is expressed in terms of the height reached by the liquid, h, surface tension of liquid, γ, density of liquid, ρ, contact angle between the liquid and capillary wall, θ, and gravitational constant, g. By making

the substitution of pressure, $P = h\rho g$, into equation 3, equation 4 is obtained.

$$Pr = 2\gamma\cos\theta \tag{4}$$

Where, $\gamma\cos\theta$ is equal to the Wilhelmy surface tension. If the wetting liquid is assumed to have a contact angle of 0 then Eq. (4) can be re-arranged in terms of the pore diameter (d), thus allowing the porosity distribution to be obtained.

$$d = \frac{4\gamma}{P} \tag{5}$$

Porosity distribution and permeability values were obtained for each of the separator papers characterised. Data was collected using a Coulter Porometer II. A sample comprising of a separator paper disc 25 mm in diameter was cut from a larger sheet using a punch. The sample was then submerged in the wetting liquid for a minimum of 2 min to allow total saturation of the pores. The wetted sample was subsequently placed into the machine, which measures flow rate with change in pressure, and measurements taken. Permeability was measured after porosity since a dry separator is required. Measurements were repeated several times for each sample and an average taken.

2.4. Diffusion

The diffusivity of battery separator papers at varying amounts of saturation was measured using a specifically designed diffusion rig. The diffusion rig consisted of three principal components, the diffusion cell, sampling valve and gas chromatograph. Fig. 1 shows a schematic diagram of the apparatus. During diffusion measurements nitrogen and oxygen flow on each side of the sample held within the diffusion cell. The oxygen side of the cell is vented to atmosphere while the nitrogen side is connected to a sampling valve. Switching the sampling valve allows gas in the sample loop, from the nitrogen side of the cell, to be directed into the gas chromatograph. The quantity of oxygen that had passed through the separator paper in the diffusion cell was determined from the detector response.

The diffusion cell was manufactured from stainless steel and is shown diagrammatically with dimensions in Fig. 2. A gas tight seal was achieved using two PTFE gaskets, which the disk of separator paper being examined was clamped between.

Four interchangeable sampling loops were used in total, one for measurements and an additional three having various

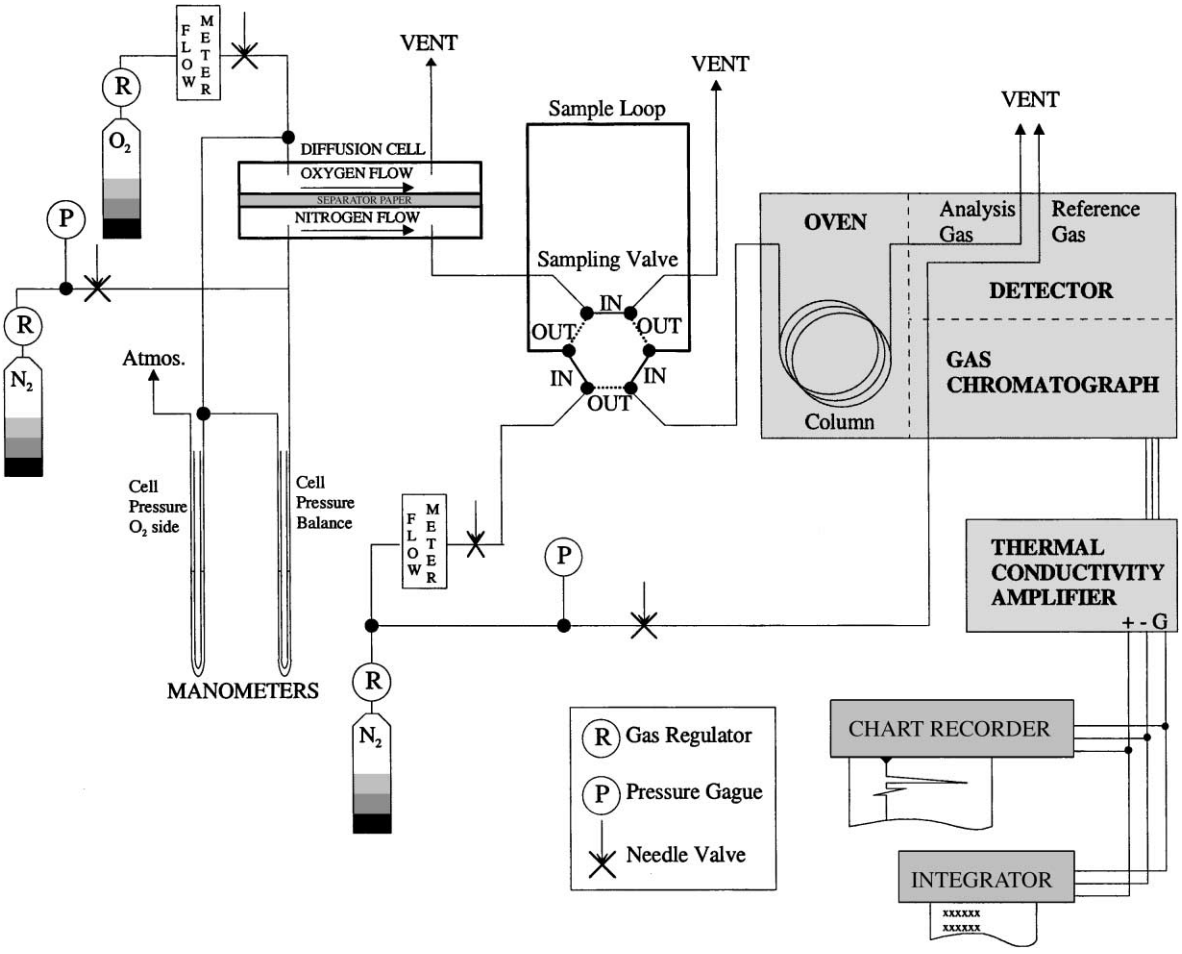

Fig. 1. Diagram of apparatus used to measure diffusivity of separator paper.

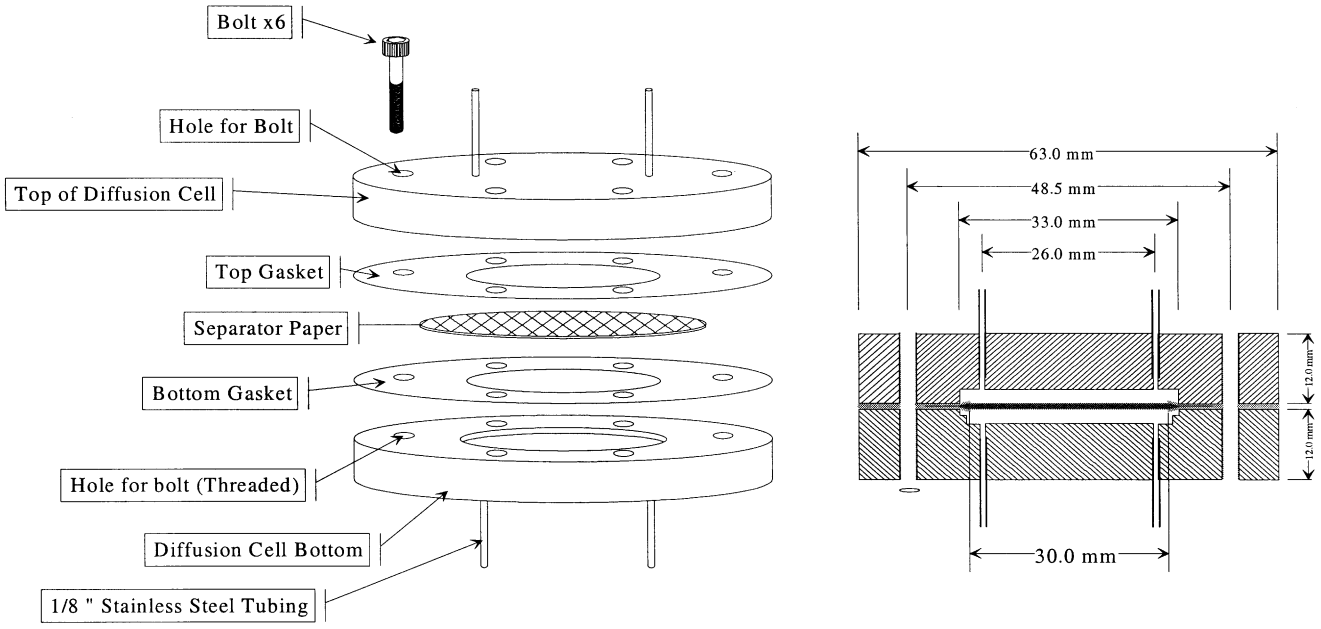

Fig. 2. Schematic diagram of diffusion cell.

Table 1
Sample loop details

Sample loop	Application	Volume (μl)
1	Measurement and calibration	490
2	Calibration	283
3	Calibration	163
4	Calibration	87

volumes for calibration purposes. Loop details are given in Table 1. Sample loops were constructed to the volumes given in the table, as these covered the range of oxygen samples expected during experimentation. The sample loop volume for measurement was 490 μl, therefore 50% is approximately 283 μl, which corresponds to the maximum theoretical volume of oxygen which could pass into the detector for an infinitely permeable sample or membrane. The 163 and 87 μl loops are approximately 66 and 33% of 283, therefore giving evenly spaced points on a calibration curve of volume of oxygen versus detector response.

A Philips PU4500 gas chromatograph was used to determine the volume of oxygen in the sample of gas. An Alltech Porapak®S washed molecular sieve column was used to separate water vapour within the sample gas which had evaporated from the sample surface. This column is traditionally used for the analysis of flue gases, but proved suitable for this application. The volume of oxygen in each sample of gas was determined using a Philips thermal conductivity detector. Due to the susceptibility of the detector filaments to oxidation the detector was operated at its minimum temperature setting. The output from the thermal conductivity amplifier was recorded using a Philips 8251 single pen chart recorder and Hewlett-Packard 3390A Integrator.

Due to sensitivity of the detector to flow rate and temperature it was necessary to calibrate the rig before each set of readings was taken. This was achieved by measuring the detector response when different volumes of oxygen gas were passed into the detector. In practice this was achieved using different sized sampling tubes and passing oxygen gas directly into the sampling valve thus bypassing the diffusion cell. Once calibrated, measurements of oxygen diffusion through the paper could be made.

2.4.1. Calculations

Due to the diffusion cell design it was not possible to constrain the surfaces of the separator once it had been inserted. A consequence of this was that the thickness of the sample could not be determined directly. When a separator paper is wetted with a liquid the surface tension causes the fibres to move together thus reducing the effective paper thickness. Because of this, the thickness of the samples whilst in the diffusion cell could only be predicted from experimental results. Measuring the thickness of a stack of each of the separator paper types examined, at varying saturations, under a constant load, allowed the separator thickness and percentage saturation of the samples in the diffusion cell to be calculated from the weight of water in the sample.

Results for each separator type examined are represented as plots of diffusivity versus percentage saturation. The volume of water in the sample, V_{H_2O}, is obtained from the weight of water in the sample using, Eq. (6). The volume of glass fibres in the sample, W_f, is obtained using Eq. (7). Percentage saturation is then calculated from the volume of water in the sample, the volume of fibres in the sample and the sample dimensions using Eq. (8). The terms used in Eqs. (6)–(8) are as follows: mass of sample, M; mass of

saturated sample before test, M_{SI}; mass of saturated sample after test, M_{SF}; weight fraction of fibre type, W_f; weight of paper per unit area (g cm^{-2}), P; density of fibre type, n (g cm^{-3}), ρ_n; sample area, A_{sample} and sample thickness obtained from experimental results, L.

$$V_{H_2O} = \frac{(M_{SI} + M_{SF}/2) - M}{\rho_{H_2O}} \quad (6)$$

$$V_{fibres} = A_{sample} \sum_n \frac{W_f P}{\rho_n} \quad (7)$$

$$\text{saturation}\,(\%) = \frac{V_{H_2O}}{(A_{sample} L) - V_{fibres}} 100 \quad (8)$$

2.4.2. Determination of separator effective diffusivity

To determine the effective diffusivity of the separator paper the mole fraction of oxygen on the nitrogen side of the cell must be calculated. The mole fraction of oxygen is obtained from the peak area, sample loop volume, and gradient, m, and intercept, c, of the calibration curve of volume of oxygen versus detector response, using Eq. (9). A diagram of the diffusion cell is shown in Fig. 3.

$$y_{O_2,L} = \frac{[(\text{peak area} - c)/m]}{\text{sample loop volume}} \quad (9)$$

Oxygen flux through the separator is calculated from (i) the mole fraction of oxygen on the nitrogen side of the cell, $y_{O_2,L}$, (ii) the flow rate of nitrogen in the cell, v_{N_2}, and (iii) the area of the separator paper exposed by the hole in the gasket, A, using Eq. (10).

$$N_{O_2} = \frac{y_{O_2,L} v_{N_2}}{A} \quad (10)$$

The ratio of the fluxes, N, of two gases on each side of a membrane is equal to the square root of the ratio of atomic masses, M [7,8]. This relationship can be used to obtain the nitrogen flux from the oxygen flux as shown in Eq. (11).

$$\frac{N_{N_2}}{N_{O_2}} = -\sqrt{\frac{M_{O_2}}{M_{N_2}}} = -\sqrt{\frac{32}{28}} = -1.07 \quad (11)$$

The mole fraction of nitrogen on the oxygen side of the diffusion cell is calculated using Eq. (12).

$$y_{N_2,0} = \frac{N_{N_2} A}{v_{O_2}} \quad (12)$$

And the mole fraction of oxygen from Eq. (13).

$$y_{O_2,0} = 1 - y_{N_2,0} \quad (13)$$

Since the gas is continuously being replaced on each side of the cell it is necessary to calculate the average mole fraction of oxygen on each side of the sample. On the oxygen side, oxygen is continuously being added, therefore the concentration increases. On the nitrogen side, nitrogen is continuously being added, consequently the concentration of oxygen decreases. Eqs. (14) and (15) are used to calculate the averages.

$$\overline{y}_{O_2,0} = \tfrac{1}{2}(1 + y_{O_2,0}) \quad (14)$$

$$\overline{y}_{O_2,L} = \tfrac{1}{2}(0 + y_{O_2,L}) \quad (15)$$

Fick's law, Eq. (16), states that the flux across a material is equal to the effective diffusivity, D_{eff}, multiplied by the concentration gradient (dC/dx).

$$N_{O_2} = -D_{O_2,eff} \frac{dC}{dx} \quad (16)$$

Concentration, C, can be related to pressure, P, by rearranging Eq. (17) to give, C in terms of, volume, V, moles, n, gas constant, R, and, temperature, T as shown in Eq. (18).

$$PV = nRT \quad (17)$$

$$C = \frac{n}{V} = \frac{P}{RT} \quad (18)$$

Eq. (18) can be substituted into Eq. (16) to give flux in terms of pressure, shown in Eq. (19).

$$N_{O_2} = -\frac{D_{O_2,eff}}{RT} \frac{dP_{O_2}}{dx} \quad (19)$$

dP_{O_2} is equal to the change in partial pressure of oxygen between the two sides of the separator paper where dx is the

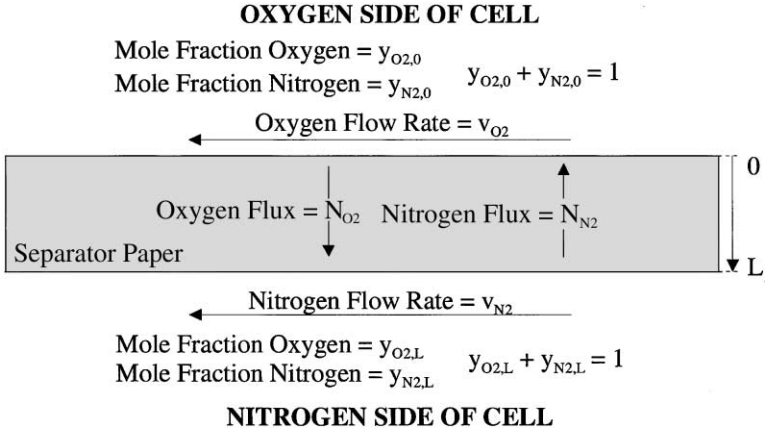

Fig. 3. Diagram of gas flows during measurement of diffusivity.

thickness of the separator, Eq. (19) can therefore be modified to give Eq. (20).

$$N_{O_2} = -\frac{D_{O_2,\text{eff}}(P_{O_2,0} - P_{O_2,L})}{RTL} \quad (20)$$

Since both oxygen and nitrogen behave as ideal gases at room temperature the partial pressure of oxygen on each side of the cell is directly proportional to the molar fraction. This allows the effective diffusivity to be calculated by substituting pressures for mole fractions and rearranging Eq. (20) to give Eq. (21).

$$D_{\text{eff}} = \frac{N_{O_2} LRT}{P(\bar{y}_{O_2,0} - \bar{y}_{O_2,L})} \quad (21)$$

2.5. Compression tests

The apparatus used to characterise the separator papers consisted of a horizontal jig mounted in an Instron mechanical testing machine. Loads were monitored using a load cell with range 0–500 N. The load cell output was recorded using a chart recorder. A diagram of the apparatus is shown in Fig. 4.

A stack of 20 sheets, each 10 cm × 10 cm, was used for each test. These dimensions were chosen since they are similar in size to the sheets of separator paper used in commercially available batteries. Separator paper was provided in the form of a roll and samples were taken in a line along the centre of the paper. Once inserted into the testing machine the stack of papers was compressed until a force equivalent to a pressure of 25 kPa was measured. This load is comparable in magnitude to that used in the manufacture of commercially available batteries. There was no significant difference in the thickness of the papers tested when under this load.

Separator papers exhibit viscoelastic behaviour, the consequence of this being a steady decrease in the force applied by the paper with time after compression had ceased. The rate of the decrease in force is directly proportional to the compression rate. For this reason a slow cross-head (loading) rate of 1 mm min^{-1} was used as this minimised the rate of reduction in force due to paper relaxation.

Following compression of the separator papers an amount of electrolyte equivalent to one-fifth of the total pore volume was added. After the electrolyte had been adsorbed into the separator paper a reading of the force was taken. Initial measurements indicated that steady state conditions were not reached after a period of more than 6 h. Waiting for this period of time has a number of disadvantages such as electrolyte evaporation. However, approximately 90% of the total change in force measured after a period of 30 min from the addition of acid occurred in the first 10 min. It was therefore decided to take measurements of force after a set time of 30 min, since after this length of time, the majority of the change in force had been observed and changes due to evaporation would be insignificant. This step was repeated allowing the force to be monitored at saturation levels of 0, 20, 40, 60, 80, and 100%.

3. Results and discussion

3.1. Scanning electron microscopy

Examination of each separator paper type showed that the papers had a rough and smooth side. Subsequent examination in the scanning electron microscope indicated that the best representation of fibre size and orientation was obtained from the images taken from the smooth side, as more fibres were within the depth of field of the microscope.

Type A glass separator paper is shown in Figs. 5 and 6 at low and high magnifications, respectively. Glass fibres range in diameter between <1 and approximately 3.5 μm. A larger proportion of the thicker fibres appear to be orientated in the

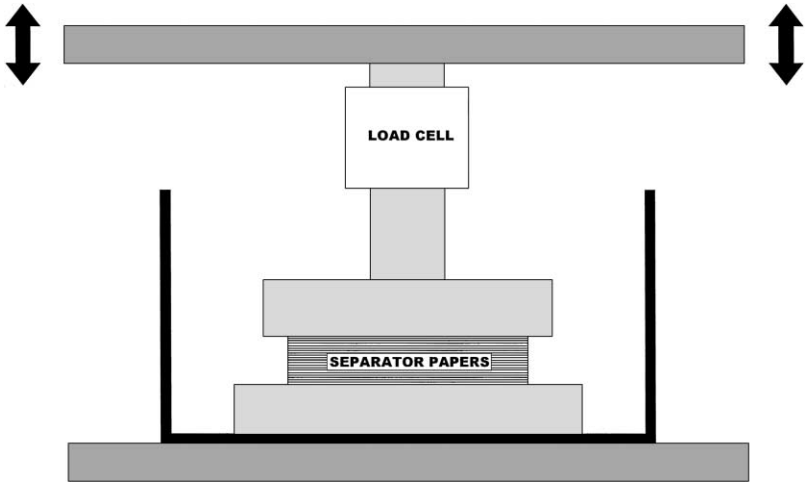

Fig. 4. Diagram of apparatus used to measure compressive properties of separator paper.

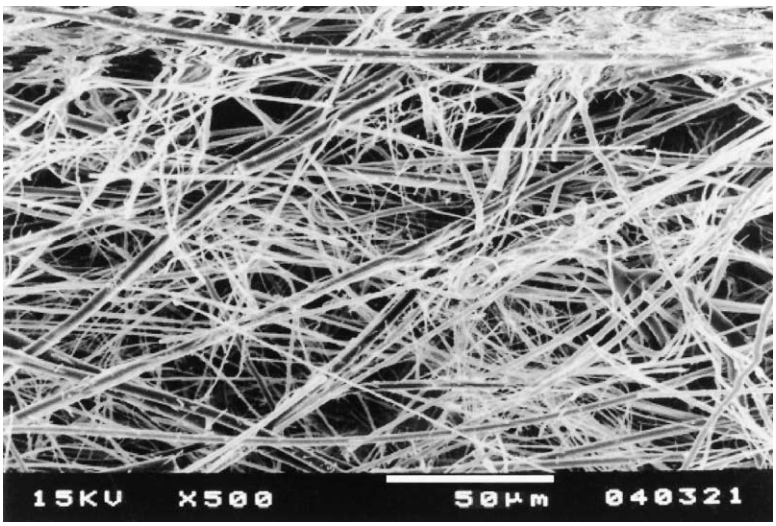

Fig. 5. Separator paper type A—low magnification.

machine direction (horizontal in figure) compared to the thinner fibres.

Images of the type B separator paper are given in Figs. 7 and 8 at low and high magnifications, respectively. Fibre diameters range between <1 and approximately 5 μm. A larger proportion of the fibres are orientated in the machine direction, compared to the other separator papers examined.

Figs. 9 and 10 show low and high magnification images of type C separator paper. Polyester fibres are visible in Fig. 10 and are identified by their thickness, which is significantly larger then that of the glass. The polyester fibres are approximately 20 μm in diameter, and the glass fibres range in size between <1 to approximately 3.5 μm. A number of the glass fibres appear to be permanently attached to the polyester fibres. Both polyester and glass fibres show random orientation in both figures.

3.2. Wicking tests

Within a battery cell, wicking rate will influence the time taken for the electrolyte to penetrate all areas after the initial acid fill. During subsequent operation the separator papers are not completely saturated allowing electrolyte to move between areas of differing saturation. Wicking tests were used to measure the speed at which electrolyte moves through the various separator papers by capillary flow.

Plots of time versus "height squared" for the separator types examined are shown in Fig. 11. When wicking height, h, is much less than the maximum wicking height h_m, a linear relationship is observed, allowing linear regression lines to be plotted between each set of data points [1]. A linear relationship is obtained for both separators containing

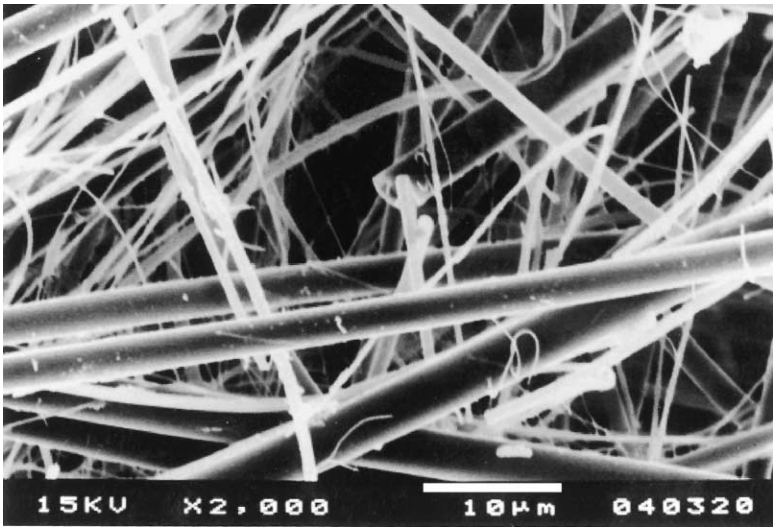

Fig. 6. Separator paper type A—high magnification.

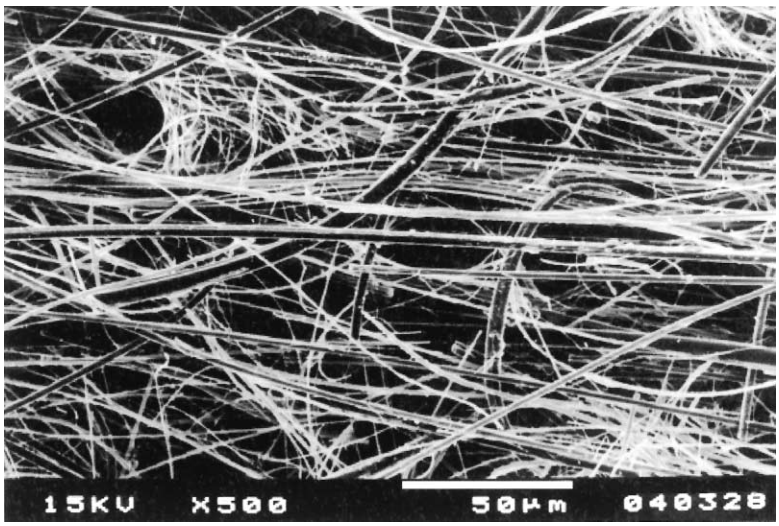

Fig. 7. Separator paper type B—low magnification.

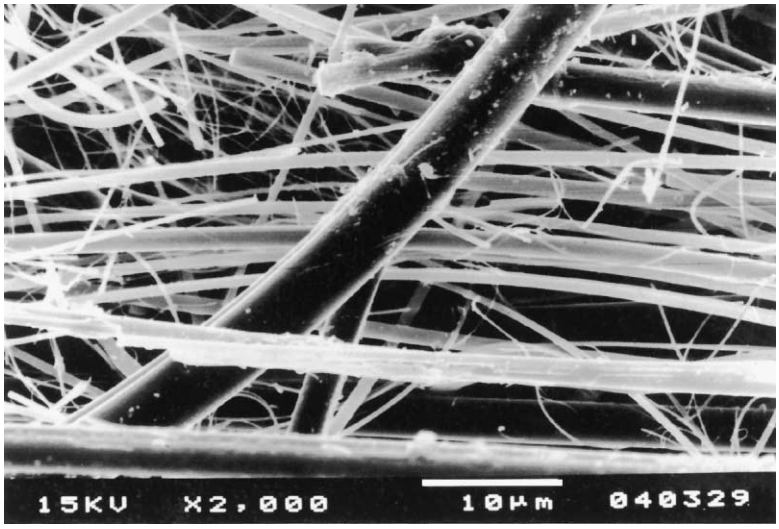

Fig. 8. Separator paper type B—high magnification.

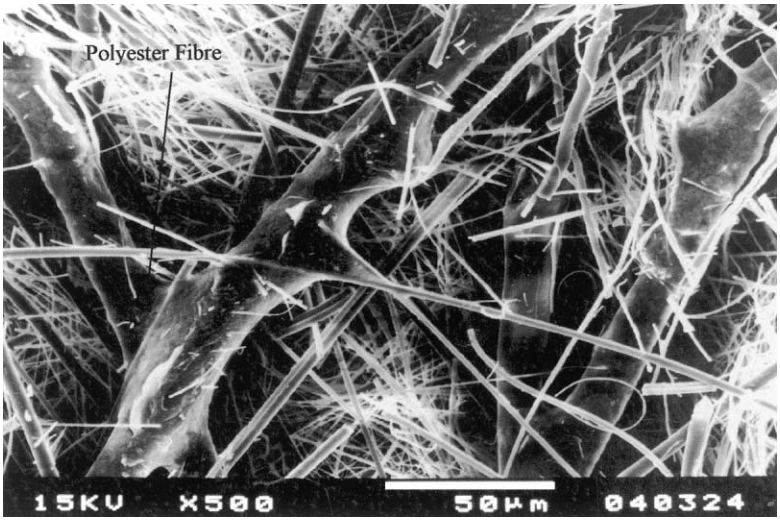

Fig. 9. Separator paper type C—low magnification.

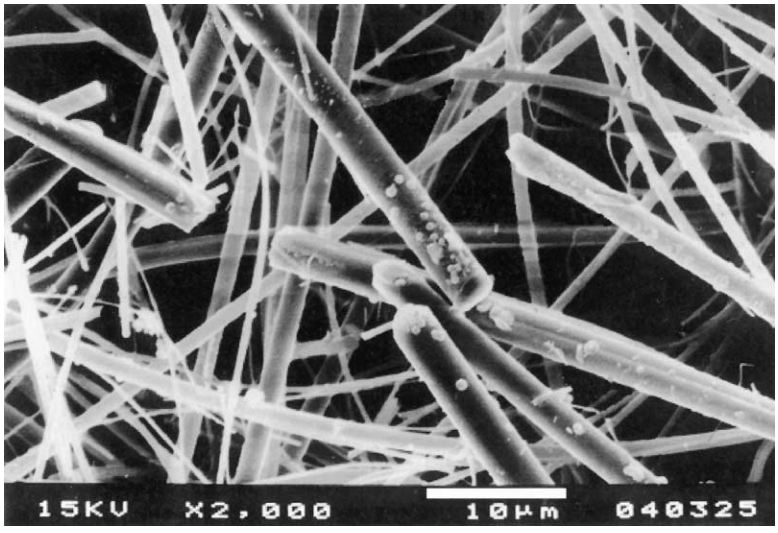

Fig. 10. Separator paper type C—high magnification.

100% glass, however a non-linear relationship is obtained for the separator containing polyester fibres. This is because the polyester fibres have a higher contact angle with sulphuric acid compared to the glass. A lower value of h_m results and the linear t versus h^2 relationship is no longer valid.

Both of the 100% glass separator papers have the highest wicking rate in the machine direction. Wicking rate will be influenced by a number of parameters such as the range of fibre diameters' [2] and fibre orientation. The average wicking rate from the two directions is greatest for the type B separator, suggesting that when saturated and unrestrained it has a larger, average pore radius, or number of pores, compared to the other papers therefore allowing maximum flow of electrolyte. The difference between the wicking rates in the 0° and 90° directions is greatest for the type B separator paper. This is a likely consequence of the higher proportion of orientated fibres, as identified by examination in the scanning electron microscope.

3.3. Permeability measurements

Permeability and porosity measurements are shown in Table 2. The lowest permeability was obtained for the separator containing polyester fibres, type C, which was just over half the value obtained for the 100% glass separators. The values obtained for the two 100% glass separators, type A and B, are very similar although the type B separator has a larger maximum pore size and a higher permeability compared to the type A separator material.

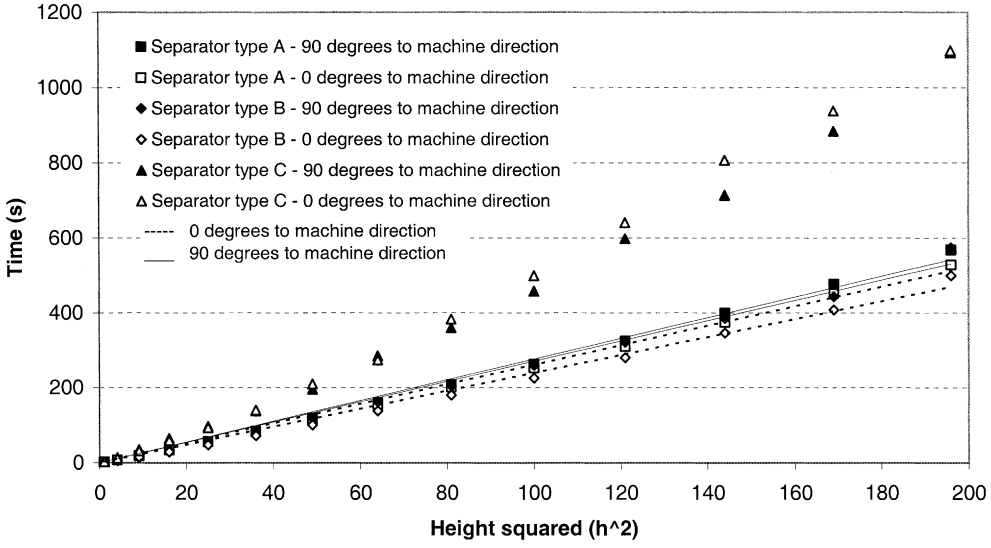

Fig. 11. Wicking rates of separator types A, B and C.

Table 2
Porosity and permeability measurements

Separator type	Porosity (μm)			Permeability (l min^{-1} cm^{-2})
	Minimum	Maximum	Mean	
A	3.9	14.4	5.8	13.2
B	4.5	14.6	6.7	14.7
C	3.0	9.0	4.6	7.9

3.4. Diffusivity measurements

During the life of a VRLA battery, water loss from the electrolyte caused by repeated charging during cycling results in the battery cell operating at an ever-decreasing level of saturation. Separator saturation will affect battery operation by influencing the diffusion of gases and ions between the positive and negative electrodes. At high saturation levels ionic conduction through the electrolyte will be high and diffusion of gases low and at low saturation levels diffusion of gases will be high and ionic conduction low. The effect of saturation on the flow of gases across the separator paper has been determined by measuring the separator diffusivity at varying saturation levels.

Diffusivity measurements have not been made for the type C polyester separator due to its unavailability, however measurements have been taken on the two 100% glass separator papers. Plots of diffusivity versus saturation for type A and type B separator papers are given in Figs. 12 and 13 below.

It can be seen that both graphs exhibit a similar trend. Each plot can be divided into three distinct sections. The first section consists of a horizontal plateau along which the diffusivity remains relatively constant up to a break point. The saturation at which this point occurs is different for the two separator papers examined. At saturation levels above the break point there is a steady decrease in diffusivity, which continues linearly until a diffusivity of zero is reached. Above this saturation the diffusivity remains at zero. This trend is similar to that observed by Culpin [9], where a rapid decrease in diffusivity was observed between saturation levels of approximately 70 and 90%.

Diffusivity of the dry separator papers is similar, around 0.01 cm^2 s^{-1} with the type B separator just above this value, and the type A below. As the saturation of the separator papers increases greater numbers of the gaps or pores between the fibres fill with electrolyte. At low saturation levels this has little effect on diffusivity. However, at higher saturation levels distinct paths through the separator are formed. As saturation increases further individual paths are blocked therefore reducing the diffusivity. This process continues until all paths through the paper are blocked and the diffusivity reaches a value of zero. Culpin [9] suggests that this trend may be a result of the anisotropic structure of the separator paper and the fact that pores in the plane of the paper are generally larger than those in the transverse direction.

Correlation coefficient values of lines plotted using a least squares fit, between the break point and zero saturation (filled points on figures), are 0.97 and 0.98 for the type A and type B separator papers, respectively. This strongly implies that the relationship is linear. The gradient of the line corresponding to the type B separator paper is half that of the type A paper, which suggests that as saturation increases the paths become blocked at a lower saturation level in the type B separator paper compared to the type A. There is little difference between the saturation levels at which the diffusivity becomes zero for both papers.

3.5. Separator paper compression tests

Compression tests, described in the experimental methods chapter, were carried out on type A and type B 100% glass separator papers in order to determine how the force that is exerted by each paper varies with electrolyte saturation. In order to do this it was necessary to compress the papers and

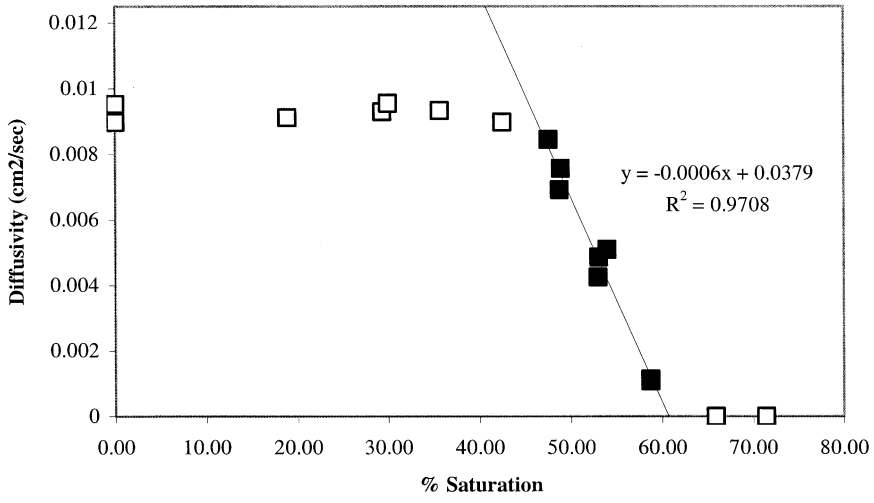

Fig. 12. Diffusivity vs. saturation for separator type A.

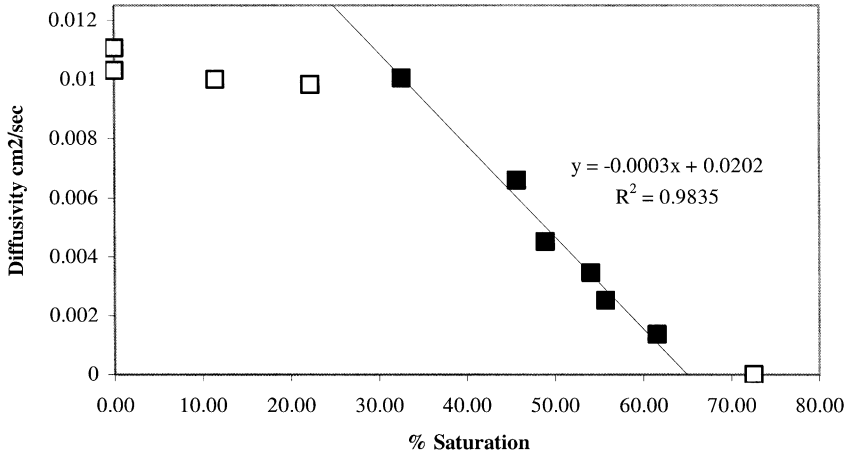

Fig. 13. Diffusivity vs. saturation for separator type B.

add electrolyte in stages taking measurements at each saturation level.

After the initial compression of both separator types in the dry condition, 0% saturation, a steady drop in force was observed. This indicated that the papers exhibit viscoelastic behaviour. Initial results showed that this produced negligible variations when readings were taken after a predefined relaxation time. There are a number of possible mechanisms that could explain this behaviour.

Since the viscoelastic behaviour of glass, below the glass transition temperature, is insignificant within the time scales of this investigation, the behaviour of the separator papers is primarily influenced by the structure rather than the compositional or material properties of glass.

Separator paper consists of a mass of fine glass fibres inter-linked in various orientations shown diagrammatically in Fig. 14. Glass is a brittle material and does not exhibit plastic deformation characteristics. During compression of separator paper the fibres will bend until they reach their elastic limit, after which fibre fracture occurs. In addition to fracture, the only way in which the fibres can release the elastic strain energy stored within them is to move into a position where the bending strain is reduced. The time response for the fibres to move is the mechanism believed responsible for the paper's viscoelastic behaviour. In practice this will be a cumulative effect of a large number of fibres moving synchronously together. The situation of two fibres acting on each other is represented diagrammatically in Fig. 15.

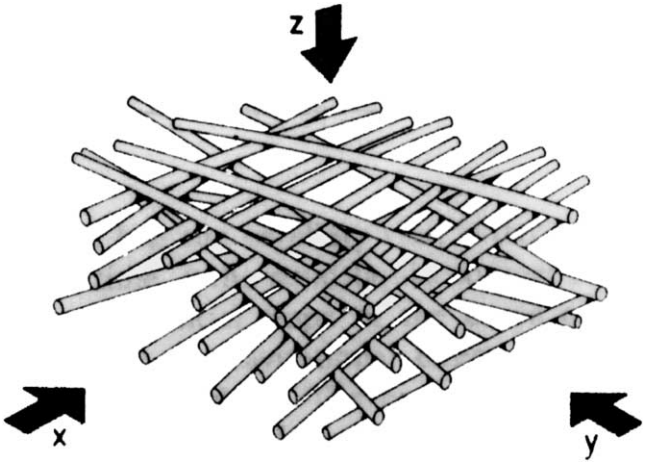

Fig. 14. Simplified structure of separator paper.

Separator papers consist of many fibres crossing each other, a pair of which is shown in Fig. 15(a). When a load is applied to the fibres, elastic deformation occurs and the fibres deform as shown in Fig. 15(b). As the strain increases

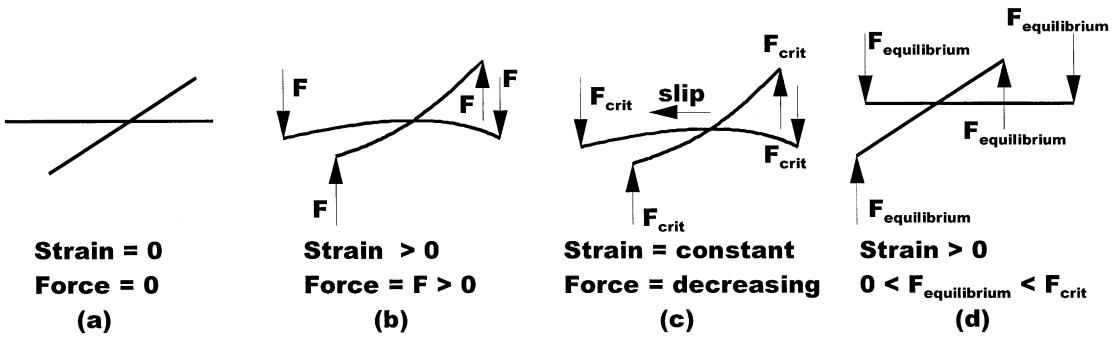

Fig. 15. Representation of fibre movement within a separator paper during compression.

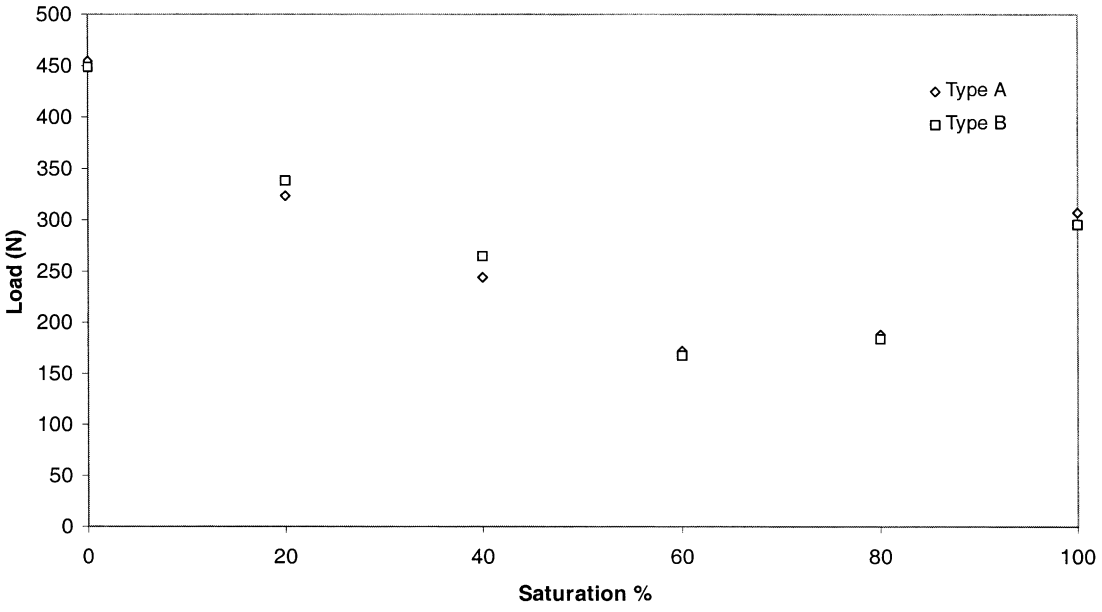

Fig. 16. Load vs. saturation for separator types A and B.

a critical force is reached at which point the fibres are able to slip past each other, resulting in a decrease in their deformation, Fig. 15(c). The effect of this is a reduction in the force exerted by the fibres, whilst maintaining the same overall separator strain. At a particular point the sliding fibres will reach an equilibrium force condition at which the sliding will stop, Fig. 15(d). The result is a decrease, from the initial force exerted by the compressed separator with time. Alternatively, if the fibres are unable to slip to a position of lesser strain, fibre breakage will occur when the force exceeds that for fracture.

In practice the mechanism described above will be influenced by other factors such as the surface tension and lubrication effects of the electrolyte. A plot of load versus saturation for both separator papers consisting of 100% glass is shown in Fig. 16.

From the figure it can be seen that there is no significant difference in the behaviour exhibited by both separator types. A decrease in force occurs between 0 and 60% saturation, followed by an increase between 60 and 100%. Investigations by Nakamura et. al. [2] indicate a similar trend when contraction percentage is plotted against amount of electrolyte added to the separator sample. This can be explained by considering the interaction between the electrolyte and fibres, shown diagrammatically in Fig. 17. From the figure it can be seen that there is no force acting between the fibres at 0 and 100% saturation. However, at an intermediate level of saturation a drop of electrolyte can sit between the fibres. The surface tension of the electrolyte causes the fibres to bend towards each other reducing any force at the ends of the fibres.

As the separator saturation increases, the ratio of each interaction type between fibres as shown in Fig. 17(a)–(c), will vary and influence the total force exerted by the paper

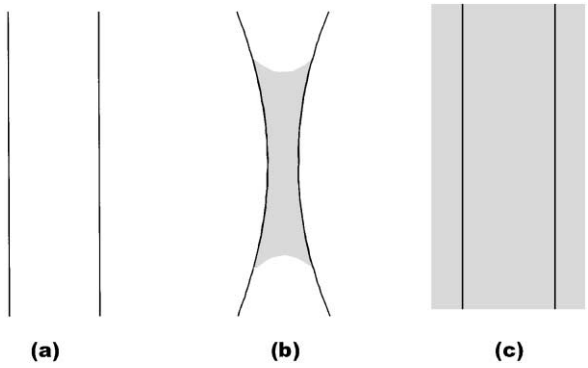

Fig. 17. Influence of electrolyte between glass fibres at 0% saturation (a), intermediate level of saturation (b), 100% saturation (c).

therefore explaining the U shape curve. It is suggested that the drop in force observed between the values at 0 and 100% saturation is due to a combination of the paper relaxation throughout the time of the experiment, lubrication of the fibres with electrolyte and surface tension effects of the electrolyte.

4. Conclusions

Scanning electron microscopy is an effective method for the examination of separator papers and allows glass and polyester fibres to be distinguished from each other. Fibre orientation has an influence on the diffusivity characteristics of partly saturated separator papers in the range 30–70% saturation. However, fibre orientation had little effect on the wicking rates and compression characteristics of the paper. The presence of polyester fibres within the paper reduced the wicking rate due to its larger contact angle compared to glass.

References

[1] B. Culpin, Separator design for valve regulated lead/acid batteries, J. Power Sources 53 (1995) 127–135.
[2] K. Nakamura, M. Shiomi, K. Takahashi, M. Tsubota, Failure modes of valve regulated lead/acid batteries, J. Power Sources 59 (1996) 153–157.
[3] K. McGregor, Effects of compression on recombant battery separator mats in valve regulated lead/acid batteries, J. Power Sources 73 (1998) 65–73.
[4] G.C. Zguris, Absorptive glass-mat separators for valve regulated lead/acid batteries—thoughts on compression, J. Power Sources 67 (1997) 307–313.
[5] G.C. Zguris, A broad look at separator material technology for valve regulated lead/acid batteries, J. Power Sources 73 (1998) 60–64.
[6] R.D. Laughlin, J.E. Davis, Text. Res. J. 31 (1961) 904.
[7] D.S. Scott, F.A.L. Dullien, Diffusion of ideal gases in capillaries and porous solids, Am. Inst. Chem. Eng. J. 8 (1) (1962) 113–117.
[8] R.B. Evans, G.M. Watson, E.A. Manson, Gaseous diffusion in porous media at uniform pressure, J. Chem. Phys. 35 (6) (1961) 2076–2083.
[9] B. Culpin, J. Hayman, Transport and wetting phenomena recombination separator systems, J. Power Sources 11 (1986).